A procedure for operational use of wave hindcasts to identify landfall of heavy swell

Valdir Innocentini[1], Ernesto Caetano[2] and Jonas Takeo Carvalho[3]

[1]Instituto Nacional de Pesquisas Espaciais, São José dos Campos, Brazil

[2]Institute of Geography, National Autonomous University of Mexico, Mexico

[3]Rede de Modelagem e Observação Oceanográfica, Centro de Hidrografia da Marinha, Niterói, Brazil

Corresponding author adress:

Dr. Valdir Innocentini, INPE, Av. dos Astronautas, 1756,

São José dos Campos - SP

Brazil

E-mail: valdir@cptec.inpe.br

(June 2013)

Abstract

The wave pattern on the Brazilian coastline is composed of both wind waves and swell. The wave systems (WSs), extracted from the spectra near the coast produced by numerical wave models, reveal the occasional presence of intense swells, with small significant wave height (H_S) and large average period (T_a). This kind of event has nearly no effect over deep water, but its landfall can be accompanied by inundation, mainly when coupled with favourable tides and storm surge. Since these events are not clearly evident in the bulk parameters, this study proposes a methodology to i) identify intense swells simulated by a coarse grid resolution wave modelling system (CWS), and to ii) evaluate their importance.

In this methodology, monitoring sites are defined along a 100-m isobath contouring the Brazilian coast, where the CWS hindcasts the spectra for a 31-year period, from 1979-2009, obtained by the WAVEWATCH wave model. The spectra are partitioned into WSs, which are used to build cumulative distribution tables (CDT) for each site. The variable used in the CDT is the flux of energy per unit length perpendicular to the wave propagation (P_W), which contains in its definition both H_S and T_a. The direction of propagation of a WS is used to compute the components of P_W parallel and perpendicular to the coast. From the CDT of the perpendicular component of P_W, the percentile of an incoming WS can be found and its intensity ranked.

To illustrate the feasibility of this proposal, the method is used to find the

50 most powerful distantly-generated swells for two sites, one on the northern and another on the southern Brazilian coast. In addition, the method is applied in two case studies, both accompanied by coastal flooding and erosion: one represents a very powerful WS arriving at the northern coast and the another a less energetic event occurring on the southeastern coast. The analysis of bulk parameters fails to identify the second case as potentially destructive, while the proposed methodology clearly gives some indication.

1. Introduction

In operational numerical weather prediction, accurate forecasting of some events demands high spatial and temporal resolution, which may be a major impediment due to high-performance computer resource requirements. A less computer intensive approach is to run a lower resolution model and to monitor the precursors of the target event. When certain specific conditions are satisfied a high resolution and accurate numerical simulation is carried out. As examples the predictive scheme for the Atlantic basin tropical cyclones, using West African rainfall as predictor (Gray and Landsea 1992), and for tornado development, where a set of observational and numerically simulated precursors is monitored (Paice 1998).

A similar situation is found in oceanic wave prediction near the coastline. Usually a coarse grid global wave modeling system (CWS) simulates the generation and propagation of the wave spectra over deep water up to the 100-m isobath following the coast. However, for accurate prediction in shallow water and areas near the coastline, a fine grid wave modeling system (FWS) with a very high bathymetric resolution and appropriate representation of physical processes is applied.

The ideal configuration should incorporate the FWS in a coastal modeling system able to combine tides, surges, waves and wave-current interaction, such as that used by Brown and Wolf (2009) in a case study of surge occuring in northwestern England. Unfortunately, in many forecasting centers, only the CWS is operationally available, and when a powerful fetch (large area with homogeneous surface wind blowing for several hours) develops near the coast and the wave model presents significant wave height (H_S) greater than about 2.5 m propagating toward the coast, the forecaster issues an warning. In general the forecast analysis is based on bulk parameters such as H_S, average period (T_a), peak period (T_p), and their respective directions, all computed from the energy spectrum, which is the wave model prognostic variable.

In countries with an extensive coastline, e.g. Brazil with more than 9000 km, it is impossible to maintain an operational coastal modeling system . A realistic and sound alternative is to develop a set of tools producing predictors and to leave the coastal system (composed of several numerical models) in stand-by mode, waiting to be activated for a critical region when necessary . However the bulk parameters, in the case of the Brazilian coast, are not sufficient either for the forecast analysis nor as a predictor for the FWS due to the complexity of incident wave systems. More suitable parameters must be extracted from the spectra.

The Brazilian coast spans latitudes 34°S to 3°N , and has a geographic configuration exposing it to waves generated by wind regimes within semi-permanent and migratory meteorological phenomena. The northern and northeastern coastlines receive the gentle nearly unchanging waves generated by the widespread fetch within the trade winds, while the semipermanent anticyclone positioned over the South Atlantic forms northeasterly waves incident on the northeastern and southeastern coast. On the other hand, migratory extratropical cyclones, in both hemispheres, generate waves incident on almost all the Brazil's coastline, except perhaps the northern part of the northeastern coast from 10°S to 5°S. The coastline facing the North Atlantic receives swell generated by distant extratropical cyclones during the North Hemisphere winter causing some damage (Innocentini et al. 1999). However, the most extreme waves are imposed by extratropical cyclones developing over the South Atlantic, so they have received more attention from researchers (e.g. Innocentini and Caetano Neto 1996; Rocha et al. 2000).

Regarding extreme events, some researchers emphasize the location of the associated extratropical cyclone. Two regions in the South Atlantic are highlighted by Sinclair (1995) as cyclogenetic, east of Argentina (45°S) and east of Uruguay (30°S). Rocha et al. (2004) studied six extratropical cyclones in 1999 developing in these two regions with the NCEP-NCAR reanalysis (Kalnay et al. 1996). The mature stage (stronger surface winds) were localized within 35°- 30°S and 45°-30°W, with east, southeast and northward trajectories. Machado et al. (2010) selected 40 extreme events with $H_S > 6$ m, very close to the south Brazilian coast, from the wave hindcast obtained using the WAVEWATCH model for the period 1979-2009: 80% of the cases are developed over the ocean just offshore of Uruguay.

Since these studies concern extreme H_S occurrences west of 30°W (not too far from the coast), the analysis of the bulk parameters is sufficient to carry out the investigation because only one wave system plays the main role in forming the wave pattern relevant to the coast.

However, a closer examination of the spectra along the southern and southeastern Brazilian coastline reveals that it is common to have two or three wave systems, one due to local wind (wind sea) and others propagating from distant regions, outside those contemplated by the cited studies.

For a fixed observer, the further away a wave system has been generated, the smaller the H_S and the larger the T_p. However, it may contain energy large enough so that H_S becomes very high when the waves are traveling over shallow water, as in a *meteorological tsunami*, but the standard analysis based on bulk parameters would hardly detect its importance. As it will be shown, a wave system with $H_S = 4$ m and $T_a = 6$ s has smaller wave power than a wave system with $H_S = 2.5$ m and $T_a = 16$ s: both cases represent favorable scenarios for damage along the coast, but in the second case (generated from east of longitude 30°W)) this is not revealed by the bulk parameters.

The main objectives of this study are i) to present a procedure to identify energetic swells simulated by a CWS propagating from a distant storm, and ii) to find cases of distantly generated strong swell reaching the Brazilian coast and to identify the associated meteorological events.

Here, the spectrum is partitioned into wave systems, which are evaluated by their wave power or energy flux. First of all, it is necessary to know the climatology of the wave systems incident on the Brazilian coast. This will be carried out in three steps: i) hindcast a database composed of spectra every 3 hours at 61 virtual sites along the 100-m isobath; ii) extract the wave systems from each spectrum, computing their properties; iii) generate percentile tables for the flux of energy. These procedures are discussed in Section 2. Section 3 presents the main features of the stronger events generated in the North Atlantic (South Atlantic) arriving at the northern (southeastern) Brazilian coast with $T_p > 15$ s. Section 4 applies the methodology to two case studies, and finally Section 5 summarizes the main results. The present paper, designated as part I, presents the basic methodology in order to illustrate its potential. In another study, part II, observations near the coast and a FWS will be used to assess the accuracy of this methodology in providing the predictors.

2. Description of the procedure

An operational scheme for numerical wave prediction can be composed of two systems of grids: a set of coarse resolution grids (CWS), where the waves are accurately simulated over deep ocean and the wind forcing is essential, and a set of finer grids (FWS), where the coastline and bathymetry are accurately represented in order to modify the waves propagating towards the coast with shallow water wave physics incorporated. Usually the grid resolutions are 0.1 - 1° (CWS) and 50-2000 m (FWS). The 100-m isobath is a reasonable reference depth for separating the two grid systems.

Since the CWS deals with global or very large domains, the WAVEWATCH III model (Tolman 2008, hereafter WW3) is used to simulate the spectral wave energy generated by the surface wind. Simulations in coastal water are required from the FWS and the SWAN model (Booij et al. 1999) provides an appropriate solution, one that has been used in many studies (e.g. Brown and Wolf 2009).

The approach adopted in this study consists of identifying signatures or key factors in energetic events simulated by the CWS having potential to cause damage to the coast. In conjunction with other predictors (e.g. tides and coastal currents) the forecasters can make decisions, as for example to trigger the FWS. The development of a tool able to evaluate the strength of an event is based on three steps: i) a long period hindcast and the definition of a set of monitoring sites along the 100-m depth isobath following the Brazilian coastline; ii) the partition of the spectra at each monitored site into WSs; iii) construction of tables with the cumulative distribution of variables computed from the WS.

a. The hindcast wave spectra and sites

Saha et al. (2010) developed a new coupled global NCEP Climate Forecast System Reanalysis (CFSR) for the period 1979-2009. The database includes ice surface coverage and 10-m winds with spatial and temporal resolutions of 0.3125° × 0.3125° and 1 h, respectively. The CFSR provides a wind forcing for wave models with a resolution higher than any previous available reanalysis. The wave hindcast is generated by the WW3 using a global domain and three nested domains, forced by the surface winds produced by the CFSR analysis for the 1979-2009 period. The global resolution is 0.625°× 0.625°and the three nested domains cover all of the Brazilian coast (Fig.1), with resolution 0.3125°× 0.3125°. The output produced by the WW3 simulations consists of average parameters extracted from the spectrum at all grid points and the spectra at 61 monitoring points along the 100-m isobath line following the Brazilian coast (Fig. 1) at 3-h intervals. The spectral database constitutes the main source for evaluating the strength of incoming wave systems with potential for causing damage to the coastline.

b. Wave system and potential significant height

Usually a spectrum is composed of several clusters or WSs, generated by different meteorological events. Many times a WS travels several thousand kilometers before reaching the coastline. There are a number of algorithms for partitioning the spectrum into WSs (Gerling 1992; Hasselmann et al. 1994; Hanson and Phillips 2001). A comparison among some of these schemes is presented by Portilla et al. (2009).

The partition of the spectrum used in this research is performed in three steps: i) identification of maxima; ii) association of spectral elements with a maximum and; iii) merging groups. A spectral element is a maximum when all surrounding elements are smaller: since the spectrum is discretized into directions and frequencies, each spectral element is surrounded by 8 elements, except those with minimum or maximum frequency which are surrounded by only 5 elements. Each maximum defines the first element of a WS, and a label is attributed to each one (e.g., 1, 2, 3, etc ...). The next step is to find the parent of each spectral element, defined as the element among its neighbors whose spectral energy is greatest; each spectral element is assigned the same label as the parent. We found that four scans (across the frequencies and directions) in searching for the parent of each element are enough to label all elements. Finally, when a WS has a very small energy content it is discarded, and if two WSs are too close they are merged following the criteria suggested by Hanson and Phillips (2001). The main differences among the methods are the merging criteria, but at this moment this is not crucial to this study.

For each WS the usual parameters are computed: significant wave height H_S, average period T_a, peak period T_p, and their respective directions. However, in order to access the energy content of a WS, the wave power P_W, defined here as the flux of energy per unit length perpendicular to the wave propagation (the rate which the wave energy is advected - see Young, 1999, page 16), is also calculated.

It is given by

$$P_W = \rho g \int_0^\infty c_g(f) E(f) df$$

where $c_g(f)$ is the group velocity, ρ the density, g the gravitational acceleration, $f(\equiv 1/T)$ the frequency, T the period, and $E(f)$ the unidimensional frequency variance density spectrum. Defining the average group velocity by

$$\overline{c_g} \equiv (1/\overline{E}) \int_0^\infty c_g(f) E(f) df$$

where

$$\overline{E} = \int_0^\infty E(f) df$$

it follows that

$$P_W = \rho g \overline{c_g} (H_S/4)^2$$

where $H_S \equiv 4\sqrt{\overline{E}}$. For deep water, $c_g = g/(4\pi f) = gT/(4\pi)$, then

$$P_W = \frac{\rho g^2}{64\pi} H_S^2 T_a$$

A similar formulation can be found in many texts, as for example Dean and Dalrymple (2003). Often P_W is expressed in the international system of units (e.g. Sasaki 2012):

$$P_W \approx 0.5 H_S^2 T_a \quad \text{[kW/m, m, s]}$$

where H_S and T_a must be expressed in meters and seconds, respectively. It must be emphasized that this relationship is true only in deep water.

For a convenient interpretation of the results, the potential significant height H_{SP} replaces the wave power. It is defined as the H_S which the WS would have if its period were 10 s. Then for a WS with wave power P_W, H_{SP} is given by

$$H_{SP} = \sqrt{\frac{P_W}{10 \times 0.5}} \quad [\mathrm{m}]$$

One needs to keep in mind that H_{SP} is just a form to express the wave power, and its value never can be compared with H_S. Therefore the choice of 10 s is arbitrary and any other value could be chosen, without any detriment to the discussion.

c. The cumulative distribution of potential significant height

In order to classify the strength of a particular WS, the H_{SP} of all WSs reported at a site must be known. The information must be organized in a database, so that the statistical percentile of the target incoming event can be determined. For this purpose, the cumulative distribution tables (hereafter CDT) are constructed for the period 1979-2009 at each site along the 100-m isobath.

More specifically, four CDTs for H_{SP} are computed for each site: according to the peak direction of a WS, H_{SP} is decomposed into components perpendicular and parallel to the 100-m isobath. Depending on its direction, the H_{SP} parallel component can be from the right or left. Here the forward direction is taken in the sense of the motion vector of the WS towards the coast. Then each computed value is tabulated with 0.1 m class intervals, and the CDTs obtained are : i) total; ii) perpendicular; iii) from the left; and iv) from the right. Cases with $H_{SP} < 0.5$m are excluded.

Note that for the WS we are using T_a to compute P_W, but the decomposition is done with T_p. Although quite distinct for the entire spectrum, they are very similar for a simple WS.

3. The generating region and characteristics of some cases

The incident H_{SP} decomposed into directions parallel and perpendicular to the 100-m isobath according to their peak frequency direction are denoted by H_{SP}^{par} and H_{SP}^{per}, respectively. The main focus is on the perpendicular component, which in principle has more potential to penetrate and affect the coastline. In this section the main properties and trajectories of the meteorological events responsible for the generation of WS incident on the north and south Brazilian coast with small H_S and high H_{SP}^{per} will be described.

a. The percentile along the coast

Fig. 2 shows the percentile of H_{SP}^{per} for the 61 sites for the period 1979-2009, following the procedure outlined in Section 2. The coastline from point 1 to 7 receives the most energetic events, 0.1 % of the cases having $H_{SP}^{per} > 5$ m. From site 8 almost to site 38, the H_{SP}^{per} with percentile 0.1 % decreases, and from site 39 on there is a small tendency towards having more energetic events. Some exceptions to these general tendencies must be mentioned, as for example around site 25, where the continental shelf extends towards the ocean (Abrolhos Banks). Sites 38 and 45 demarcate the boundary between two different wave climate regimes where WSs are more energetic - more southern sites are associated with the proximity of cyclogenesis regions of the South Atlantic, meanwhile the reason for most energetic events toward the north is not immediately evident and research is required (this is beyond the scope of this paper).

b. The 50 most intense events for sites 22 and 47

The evolution of a WS generated near a site is characterized by an initially small T_p increasing as the WS becomes more energetic. In contrast, a distantly generated WS is identified first by a high T_p, which decreases slowly as the energy associated with smaller periods arrives. As a general rule, the further away the WS has been generated the slower the decrease of T_p, and for a distantly generated WS T_p remains nearly constant. Since the main interest here concerns cases that are distantly generated, the highest H_{SP}^{per} with $T_p \geq 15$s will be selected. Only cases at sites 22 and 47 will be presented, since their locations seem to be representative of incident swells from the South and North Atlantic, respectively.

Often the arrival of a WS with $T_p \geq 15$ s is observed at a certain time, but does not maintain this characteristic over the next 3 h, that is, $T_p < 15$ s. This means the WS was not generated so far way or else it merged with another WS. For this reason, a WS will be selected only when T_p remains smaller than 15 s for a time period equal or greater than 9 h.

Fig. 3 shows H_{SP}^{per}, H_S, and H_{SP} for the strongest H_{SP}^{per} events for both sites. At site 22, in general, H_S and H_{SP} are much larger than the respective H_{SP}^{per}, whereas at site 47 H_S is smaller and H_{SP} greater than H_{SP}^{per}. This means that the perpendicular wave power is better configured for 47, because for site 22 a large quantity of parallel energy flux is present. This is an expected result since the parallel energy at 47 is mainly due to the trade winds, which are persistent but not as strong as the winds in the South Atlantic for an extratropical cyclone developing near the coast, thus site 22 receives a substantial amount of parallel energy from the south.

Comparing the two sites, H_{SP}^{per} is larger for 47, which is due to its privileged location in receiving perpendicular energy from distantly generated WS comming from the North Atlantic.

c. The trajectories of some events

A detailed examination of the WSs presented in Fig. 3a revealed some with high H_S generated west of longitude 30°W, e.g. cases 5, 6, 8, etc. Certainly, they could be very easily detected by the bulk parameters. There were also other cases generated very far from site 22, but they merged during the propagation with nearby generated WS losing the characteristics of a distantly generated swell. However, from the detailed examination, cases were obtained with percentile of H_S greater than 20%, corresponding to $H_S \leq 1.8$ m for site 22, generated eastward of longitude 30°W and reaching the site without having been contaminated by nearby generated WS. Inspection of Fig. 3a reveals 15 cases satisfying this condition, whose main properties are listed at Table 1.

The location of site 22 is more likely to receive higher H_{SP}^{per} from meteorological events developing further north over the Atlantic. During the months November, December and January no WS is reported in Table 1, because during this period the energetic meteorological events developed at higher latitudes.

The trajectories of these 15 cases were tracked through the region where the winds were greater than 20 m/s, and the position of the centre of the area with stronger winds is depicted in Fig. 4. Each trajectory is labeled with the event number indicated in Table 1. Most of the cases have their entire trajectory eastward of 30°W, except events 41 and 43. The most distant event is 29, occurring on June 2007.

A quite distinct situation is observed at site 47, because all events selected are distantly generated, without the necessity of the imposition of an additional filter for H_S. Table 2 presents the main features of the 10 strongest WSs shown in Fig. 3b, and their trajectories in Fig. 5. From Fig. 3b, events 1 and 2 were the most powerfull not only for H_{SP}^{per}, but also for H_S. The trajectory of the associated fetch revealed both translating northwards. The final stages of the trajectories in Fig. 5 were reported eastward of longitude 50°W. The trajectories westward of this longitude are associated with smaller H_{SP}^{per}. For example, events 37 and 48 in Fig. 3b presented very high H_S, but small H_{SP}^{per}, and a closer examination in both cases revealed that their most energetic phase was westward of longitude 50°W (not shown).

4. The method applied to two illustrative cases

As outlined in the previous section, the analysis based on percentiles of WSs is a useful tool to identify and evaluate events with low H_S, but high T_p so the wave power is high. In particular the component H_{SP}^{per} was emphasized, since it represents the energy that can cross the shallow bathymetry and reach the coastline. Thus the objective here is focused on the wave power of a WS, which is often ignored in the evaluation of wave events.

In this section a set of procedures is described and applied to two special cases, one reaching the northern and other the southern Brazilian coastline. Both cases represent waves distantly generated by extratropical cyclones. Although there are no observational data available to confirm their importance, both cases were widely commented upon by the media. Briefly, they are:

- Case 28 March 2011: associated with erosion and inundation on the coast around site 22;
- Case 15 January 2013: responsible for the sinking of at least 5 boats on the northern Brazilian coast and inundation around site 47.

It is shown that the standard analysis based on bulk properties computed from the spectrum may fail in the identification of an energetic swell. An alternative approach, proposed to access the swell strength near the coastline, is applied in both cases. The strategy to evaluate the events is composed of these three steps: i) description of both spatial distribution and time evolution of bulk parameters at the target site; ii) discussion of Hovmöller diagrams; iii) examination of development of WSs at the target site and identification of the strongest ones.

a. The case of 28 March 2011

The importance of this case resides mainly in the erosion damage with extensive inundation along the coastline near site 22 reported by the media.

1) GENERAL DESCRIPTION

At 2100 UTC 28 March 2011 a large area with $U_{10} > 24$ m s^{-1} with direction towards the Brazilian coast was identified (Fig. 6). The distance of this fetch to site 22 was about 3,700 km. The fetch with $U_{10} > 24$ m s^{-1} traveled through the area encompassed by latitudes 45° and 35° S, and longitudes 10° W and 0° during a 54-hour period, from 2100 UTC 27 to 0300 UTC 30 March 2011. Afterwards, the wind speed decreased while the core moved eastward, stopping the process of intense wave growth. In the generating area H_S increased to more than 10 m at 0600 UTC 29 March with average direction towards the Brazilian coast, as shown in Fig. 7 where the H_S contour and mean wave vector are depicted. Since the generating wave area was far away, only swell could be expected at site 22.

Fig. 8 presents the time evolution of T_p and H_S at site 22. As one can observe, H_S presents a small rise late on 01 April, however the presence of swell is evidenced by an abrupt jump of T_p to 15 s. Further insight can be obtained from the spectrum, represented in Fig. 9 at 1800 UTC 01 April. The spectrum is composed of at least 4 WSs, but the one propagating from the southeast with $T_p = 15$ s was responsible for the coast damage.

For decision makers any harmful consequence of this swell was not evident from the analysis of the standard parameters. The evolution of the swell, while propagating from the 100-m isobath towards the coast, is determined by the bathymetric configuration and only a finer resolution wave model is able to realistically reproduce the swell modification over that region and its landfall impact. Thus, further information about the spectra is required to assess the importance of this event.

2) THE HOVMÖLLER DIAGRAM

An efficient method for assessing a general picture about the wave conditions along the cost is the use of the Hovmöller diagram for all variables. In particular, when applied to H_{SP}^{per} and its percentile, an interpretation is obtained that gives insight about the wave regarding the eventual propagation towards the coastline. As a first attempt a rough overview can be useful with this variable computed using the average H_S^{per} and T_p from the full spectrum. In general, one can expect this procedure to result in H_{SP}^{per} greater than those from individual WS, but it will indicate if further analysis is necessary. Fig. 10 presents the Hovmöller diagram for these two variables produced by the WW3 for a forecast period extending to 5 days - the vertical dashed line at 00 UTC 30 March separates the first day forecast from the previous period. The figure does not show high H_{SP}^{per} in locations around site 22, but the percentile became smaller than 6% late on 01 April, indicating that individual WSs deserve more careful and detailed examination.

3) THE EVOLUTION OF THE WS

Fig. 11 presents the evolution of H_{SP}^{per} for individual WSs at site 22 for a 4-day period beginning 30 March. The horizontal line indicates the percentile of the maximum H_{SP}^{per} obtained. The partition at each time is carried out by the method presented in Section 2. Two WSs at consecutives times are connected if the direction and T_p differences are less than 20° and 10%, respectivelly.

By 1200 UTC 01 April a WS with $H_{SP}^{per} = 0.9$ m struck site 22 and became strongest early on 02 April, with a percentile of 4.7% However these results are not sufficient to explain the inundation reported at this site. Others properties that could play a relevant role in increasing the water level must be considered, namely wind, surface pressure, and tides. An inspection of the wind and surface pressure fields reveals that they were very weak around site 22 and unlikely to contribute to enhancing the water level (not shown). However, the tide was rising and near its maximum level of about 0.7 m on 01 April (not shown), therefore its constructive combination with the distantly generated swell seems to provide the additional ingredient for the inundation and erosion reported in the coastal area behind site 22.

b. The case of 15 January 2013

This case was reported by the media as very destructive, responsible for several kinds of damage along a large section of the coast around site 47. Despite the great distance between the wave generating area and this site (near 6000 km), the winds were very strong, and thus powerful WSs hit the northern Brazilian coast with pronounced strength.

1) GENERAL DESCRIPTION

On 10 January 2013 an extratropical cyclone crossed the east coast of North America near 43°N 70°W, and moved slowly eastwards while a prominent fetch with wind speeds higher than 20 m s^{-1} was spawned over a large area. During a 24-h period, from 00 UTC 11 January, the winds were higher than 24 m s^{-1} blowing south-southeastward. Fig. 12 presents the wind fields at 1800 UTC 11 January, with a large fetch on the left flank of the cyclonic circulation.

The cyclonic circulation remained anchored nearly at the center of the North Atlantic during its life-cycle, while the sea surface wave energy increased substantially in response to such strong winds. The maximum H_S were higher than 12 m at 0900 UTC 12 January (Fig. 13). Over the following days a large quantity of wave energy propagated towards the north Brazilian coast.

The time evolution of T_p, H_S, and U_{10} at site 47 can be examined in Fig. 14. The abrupt jump of T_p early on 15 January shows the swell's arrival - note $T_p > 15$ s for a period of about 40 h. During nearly all of 16 January the persistence of $H_S > 3$ m indicates a very high flux of energy.

The spectral distribution of energy was at its maximum intensity at 0600 UTC 16 January when $H_S = 3.16$ m (Fig. 15). A weaker west-northwesterly WS with $T_p < 10$ s is due to the trades, while another stronger is propagating from the extratropical cyclone located in the North Atlantic, with $T_p > 15$ s. This description is enough to conclude that this is a very powerful WS, however further detailed analysis is necessary to reveal its importance.

2) THE HOVMÖLLER DIAGRAM

The diagram represented in Fig. 16 shows a large H_{SP}^{per} striking site 60 late on 14 January. Since this site is further north, it is one of the first to receive the swell. During the next 48 hours $H_{SP}^{per} > 2.5$ m spreads eastward along the northern Brazilian coast. The percentile $< 1\%$ evidences the powerful nature of this event.

3) THE EVOLUTION OF THE WS

The evolution of the WSs composing the spectrum from 13 to 16 January 2013, can be examined in Fig. 17. The stronger WS arrived at site 47 early on 15 January, and H_{SP}^{per} increases during the next 24 hours. The peak value was 2.8 m at 0900 UTC 16 January, corresponding to a percentile $< 0.1\%$. Certainly, this description provides very reliable information for disseminating a warning.

5. Summary and conclusions

Several operational forecasting centers produce daily bulletins reporting sea surface waves and issue warnings in case of intense events over the open sea or of shoreline flooding based on the analysis of numerical simulations. For open sea, where the seafarers are the main interested parties, a standard procedure is adopted, which consists of monitoring the behavior of averaged (or bulk) parameters computed from the simulated wave spectrum, e.g. significant wave height (H_S), average period (T_a), and peak period (T_p). In shallow water near the coast a more complex procedure must be implemented, including tides, storm surge caused by wind and sea level pressure, coastal circulation, and near shore shallow water wave forecasting. Large computational power is necessary for an extensive coastline, because the appropriate models require high resolution grids.

To save computer time and to provide guidance for the warning service for shallow water, the search of precursors indicating a possible incidence of high waves on the coast is a useful tool. However the analysis of the bulk parameters does not reveal the potential increase of the waves while propagating over shallow water. A more suitable variable is the flux of energy, or wave power, defined in deep water as $P_W = 0.5 H_S^2 T_a$. Since it contains both H_S and T_a. Large T_a is the signature of an energetic swell, which can have increasing H_S as it propagates over shallow water. Also, the spectrum is formed by several wave systems (WS), some of which are propagating parallel to the coast and are less likely to reach the coast. Then, to evaluate P_W individually for each WS, selecting the most likely to propagate towards the coast, gives a better way to search for precursors.

In this study, a methodology to evaluate the strength of a WS and its use as a precursor of coastal monitoring through the results of numerical forecasting obtained by the model WAVEWATCH is presented and is applied to the Brazilian coast.

Initially, a set of monitoring sites is defined, located on an isobath where the incident waves have suffered small influence of the seabed topography; for the Brazilian coastline 61 sites, about 100 km apart, were chosen on the 100-m bathymetric depth contour. On these sites the spectra produced by WAVEWATCH are separated into WSs, and their properties are evaluated. In order to facilitate the interpretation, the wave power is replaced by a new variable, potential significant wave height (H_{SP}), defined as the significant height for the same P_W, but with $T_a = 10$ s, i.e., $H_{SP} = [P_W/(0.5 \times 10)]^{0.5}$. Additionally, according to the peak period direction of the WS, H_{SP} is decomposed into perpendicular (H_{SP}^{per}) and parallel (H_{SP}^{par}) directions relative to the 100-m isobaths orientation.

The spectra for the sites from 1979 to 2009, provided by WAVEWATCH forced by the surface wind fields from the global NCEP Climate Forecast System Reanalysis (CFSR), were partitioned into WSs. Then, for each site, cumulative distribution tables (CDT) were constructed for the WSs, so any event can be ranked and its relative importance expressed by percentiles.

The methodology were applied with two objectives: i) to detect distantly generated WS reaching the Brazilian coast within the 31-year period run, and ii) to evaluate the strength of incident WS in an operational service.

For the first objective, two sites with quite different locations were selected, one exposed to meteorological events developing over the Central and South Atlantic Ocean (site 22, at 22.09S-319.93E), the other developing over the North Atlantic Ocean (site 47, at 2.23S-320.04E). All WSs simulated by the long-period run, arriving at these two sites with $T_p > 15$ s during a period of at least 9 hours, were selected and ordered by the value of H_{SP}; the 50 strongest cases were examined. For site 22 it was found that many cases were not distantly generated. However, when an additional filter was imposed in the form of percentile of significant wave height H_S greater than 20% (corresponding to $H_S < 1.8$ m for this site), only distant cases remained: the associated fetches (defined as a large area with $U_{10} > 20$ m s^{-1}) arose south of 39°S and west of 40°W. For site 47 this additional filter was not necessary, because on the northern Brazilian coastline all of the swells are due to distant fetches. Therefore, on coastlines exposed to several kinds of meteorological phenomena, the analysis of H_{SP} may not be enough to point to distantly generated swell, and an additional filter would be required.

For the second objective, the feasibility of applying the proposed methodology operationally was illustrated in two cases. Unfortunately wave data near shore along the Brazilian coast are rarely available, and the criterion used for choosing these cases was the damage reported by the media. The case of 28 March 2011 corresponds to an extratropical cyclone developing over the South Atlantic; the waves simulated by WAVEWATCH arrived at site 22 with $H_S = 2.0$ m, but $H_S > 10.0$ m in its generating area, about 3700 km away. Although H_S is small, $T_p > 15$ s at this site suggested this is a strong event, so further analysis based on the wave power was necessary. Therefore the spectrum was decomposed into several WSs, and the strongest achieved a maximum of $H_{SP}^{per} = 1.4$ m, corresponding to a percentile of 4.7 %.

The case of 15 January 2013 represents an extratropical cyclone intensifying over the North Atlantic: WAVEWATCH simulated $H_S > 12.0$ m over a distant region about 6000 km from site 47, which arrived at this site with $H_S > 3.0$ m and $T_p > 15$ s. The Hovmöller diagrams for the 5-day forecast of bulk H_{SP}^{per} showed percentiles smaller than 1%, but the decomposed spectrum revealed a WS even stronger, with $H_{SP}^{per} = 2.9$ m, corresponding to a percentile smaller than 0.1 %.

In cases of flooding, the occurrence of storm surge and tide must be considered, since they can accentuate the effect of the wave attack into the coastline. A closer inspection showed that in the first case (28 March 2011), the perpendicular wave power alone did not explain the inundation reported at site 22, but the tide seems to have played a crucial role. In contrast, the inundation reported in the second case (15 January 2013) was explained just by the percentile of the perpendicular wave incidence.

From this study, one may conclude that the CDT of H_{SP}^{per} and its percentiles are useful tools to access the strength of a WS. They can be used as precursors of floodings along a coastline, but the definition of threshold values will depend on other properties, that is, even with small H_{SP}^{per} a flooding can occur when other effects (e.g. storm surge or tide) are contributing to increasing the water level near the shore. The determination of the threshold percentile of H_{SP}^{per} depends on an extensive knowledge of the region considered, which is possible through observations and simulations on the nearby coast.

A possible limitation of this work is the emphasis given to the flux of wave energy perpendicular to the coast. Since there may be events at some sites where the parallel propagation is refracted locally towards the coast, resolving these cases would require more detailed knowledge of the local features of each site.

Acknowledgments. We thank Dr. Peter Caplan for his comments and suggestions for improving the English version of this manuscript. This research was supported by Fundação de Amparo à pesquisa do Estado de São Paulo (FAPESP), grant 2005/59438-9.

References

Booij, N., R. C. Ris, and L. H. Holthuijsen, 1999: A third-generation wave model for coastal regions, Part 1, Model description and validation. *J. Geophys. Re*s., **104**,C4, 7649-7666.

Brown, J. M., and J. Wolf, 2009 : Coupled wave and surge modelling for the eastern Irish Sea and implications for model wind-stress. *Continental Shelf Research*, **29**, 1329-1342.

Dean, R. and R. Dalrymple, 2003: Water wave mechanics for engineers and scientists. Singapure, World Scientific, **2**, 353 pp.

Gerling, T. W., 1992: Partitioning sequences and arrays of directional wave spectra into component wave systems. *J. Atmos. Ocean. Techn.*, **9**, 444-458.

Gray, W. M., and C. W. Landsea, 1992: African rainfall as a precursor of hurricane -related destruction on the U.S. East Coast. *Bull. Amer. Meteor. Soc.*, **73**, 1352-1364.

Hanson, J. L., and O. M. Phillips, 2001: Automated analysis of ocean surface directional wave spectra. *J. Atmos. Ocean. Techn.*, **18**, 277-293.

Hasselmann, S., K. Hasselmann, C. Bruning, and G. Komen, 1994: Extraction of wave spectra from SAR image spectra, in dynamics and modeling of ocean waves. England: Cambridge Univ. Press, Cambridge.

Innocentini, V., S.C.S.C. Prado, C.S. Pereira, F.O. Arantes, and I. N. Brandao, 2001 : Ocorrencia de vagas no arquipelago de Sao Pedro e Sao Paulo: caso outubro de 1999 *Revista Brasileira de Meteorologia*, **16**, 177-186.

Innocentini, V. and E. S. Caetano Neto, 1996: A case study of the 9 August 1988 South Atlantic storm: numerical simulations of the wave activity. *Wea. Forecasting*, **11**, 78-88.

Kalnay, E., and Coauthors, 1996: NCEP/NCAR 40-Year Reanalysis Project. *Bull. Amer. Meteor. Soc.*, **77**, 437-471.

Machado, A. A., L. J. Calliari, E. Melo, and A. H. F. Klein, 2010: Historical assessment of extreme coastal sea state conditions in southern Brazil and their relation to erosion episodes. *Pan-American Journal of Aquatic Sciences*, **5**, 277-286.

Paice, N., 1998: Autumnal funnel clouds over west Hampshire: A precursor to wintertime tornadoes. *Weather*, **53**, 419-424.

Portilla, J., F. J. Ocampo-Torres, and J. Monbaliu, 2009: Spectral partitioning and identification of wind sea and swell. *J. Atmos. Oceanic Technol.*, **26**, 107-122.

Rocha, R. P., S. Sugahara, and V. Innocentini, 2000: Marine cyclones over South Atlantic Ocean during 1999 winter. Part I: Their structure, intensity and evolution. *Preprints, Sixth Int. Conf. on Southern Hemisphere Meteorology and Oceanography*, Santiago, Chile, Amer. Meteor. Soc., 200-201.

Rocha, R. P., S. Sugahara, and R. B. Silveira, 2004: Sea waves generated by extratropical cyclones in the South Atlantic Ocean: Hindcast and validation against altimeter data. *Wea. Forecasting* **19**, 398-410.

Saha, and Coauthors, 2010: The NCEP Climate Forecast System Reanalysis. *Bull. Amer. Meteor. Soc.*, **91**, 1017-1058.

Sasaki, W., 2012: Changes in wave energy resources around Japan. *Geophysical Research Letters*, **39**, n/a-n/a.

Sinclair, M.R., 1995: A climatology of cyclogenesis for the Southern Hemisphere. *Mon. Wea. Rev.*, **123**, 1601-1619.

Tolman, H.L., 2008: User manual and system documentation os WAVEWATCH III version 3.14. NOAA/NWS/NCEP/MMAB Technical note **278**, 194 pp.

Young, I.R., 1999: Wind Generated Ocean Waves, Volume 2, Elsevier Ocean Engineering Book Series, 288 pp.

List of Figures

FIG. 6. Contours of surface wind speed U_{10} (m s^{-1}) and streamlines at 2100 UTC 28 March 2011.

FIG. 7. Significant wave height H_S (m) and mean wave direction at 0600 UTC 29 April 2011.

FIG. 8. Time evolution of significant wave height H_S (m), wind speed U_{10} (m s^{-1}), and peak period T_p (s) at site 22, from 30 March to 03 April 2011.

FIG. 9. Spectrum for the site 22 at 1800 UTC 01 April 2011. The units are m^{2}s rad^{-1}. The plotting interval is 0.1, 1, and 10 for contours smaller than 1, 10 and 100, respectively. The circle represents the period (s). The convention for propagation direction is from the center towards the plotted contour.

FIG. 10. Hovmöller diagram for the 61 sites of the perpendicular component of the potential significant height H_{SP}^{per} (m), from 28 March to 03 April 2011, in (a) meters and (b) percentile (%). The vertical dashed line delimits the forecast period, starting at 00 UTC 30 March 2011.

FIG. 11. Time evolution of the perpendicular component of the potential significant height H_{SP}^{per} (m) for individual wave systems (WS), from 30 March to 02 April 2011. The horizontal dashed line indicates the percentile of the strongest H_{SP}^{per} during the 4-day period.

FIG. 12. Wind field U_{10}, as in Fig. 6, but at 1800 UTC 11 January 2013.

FIG. 13. Significant wave height H_S, as in Fig. 7, but at 0900 UTC 12 January 2013.

FIG. 14. Time evolution as in Fig. 8, but at site 47, from 13 to 17 January 2013.

FIG. 15. Spectrum as in Fig. 9, but for the site 47 at 0600 UTC 16 January 2013.

FIG. 16. Hovmöller diagram for H_{SP}^{per} and its percentile, as in Fig. 10, but from 12 to 18 January 2013. Forecast starting at 00 UTC 14 January 2013.

FIG. 17. Time evolution of H_{SP}^{per} for the wave systems, like Fig. 11, but at site 47 from 13 to 16 January 2013.

List of tables

Figures

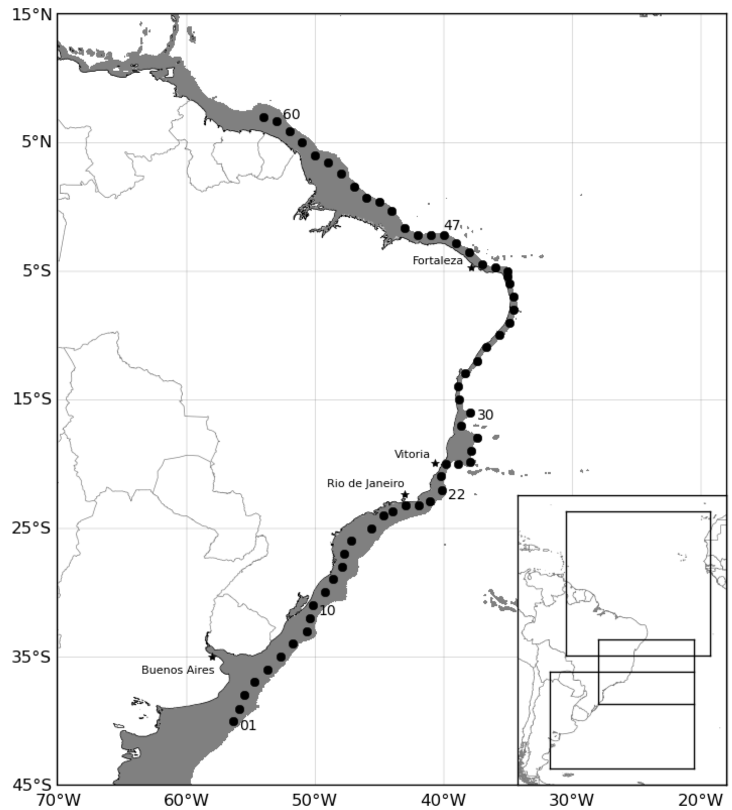

FIG. 1. The 3 domains nested into the global domain used by the WAVEWATCH simulations to build the 31-year database, and the location of 61 monitoring sites, lying nearly on the 100-m isobath following the Brazilian coastline. Areas shallower than 1000 m are represented by gray. The spatial resolution is $0.625^{\circ} \times 0.625^{\circ}$and $0.3125^{\circ} \times 0.3125^{\circ}$for the global and nested domains, respectively.

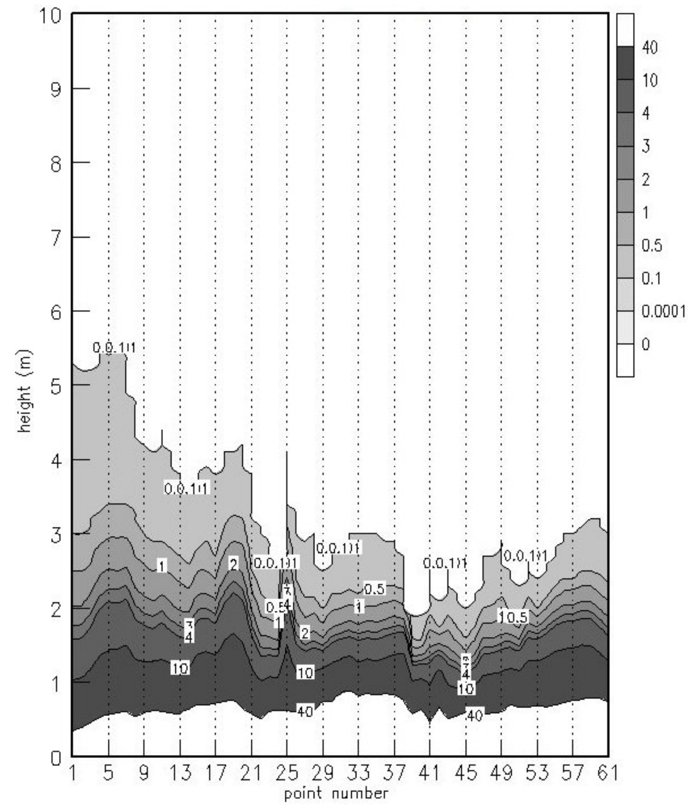

FIG. 2. The percentile (contour in %) of the 61 sites for the component of the potential significant height perpendicular to the 100-m isobath at each site (H_{SP}^{per}), computed from the 31-year database.

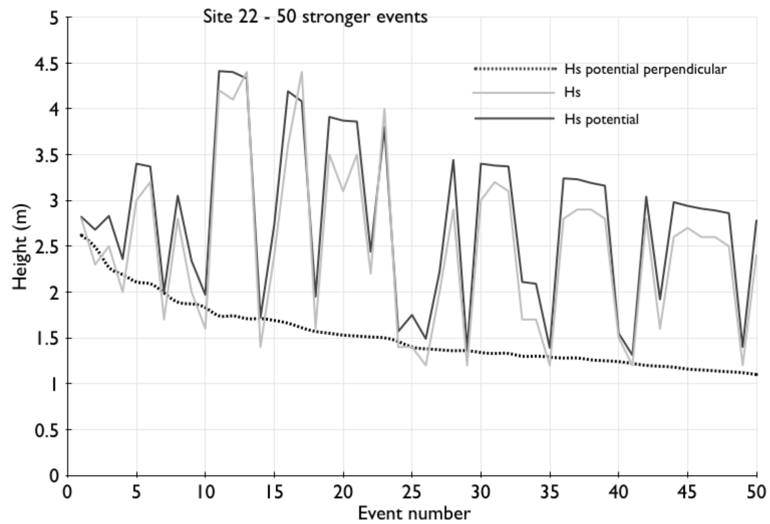

FIG. 3a

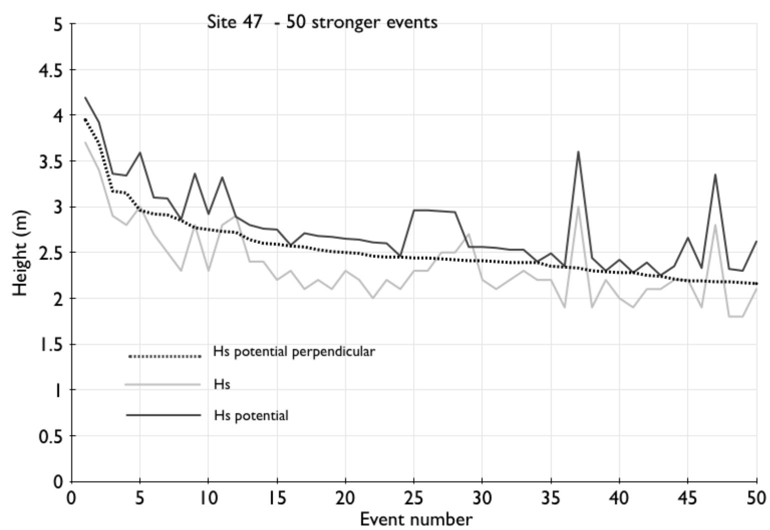

FIG. 3b

FIG. 3. Significant wave height (H_S), potential significant wave height (H_{SP}), and its component perpendicular to the coast (H_{SP}^{per}), for the 50 highest H_{SP}^{per} simulated for sites (a) 22 and (b) 47. The units are meters.

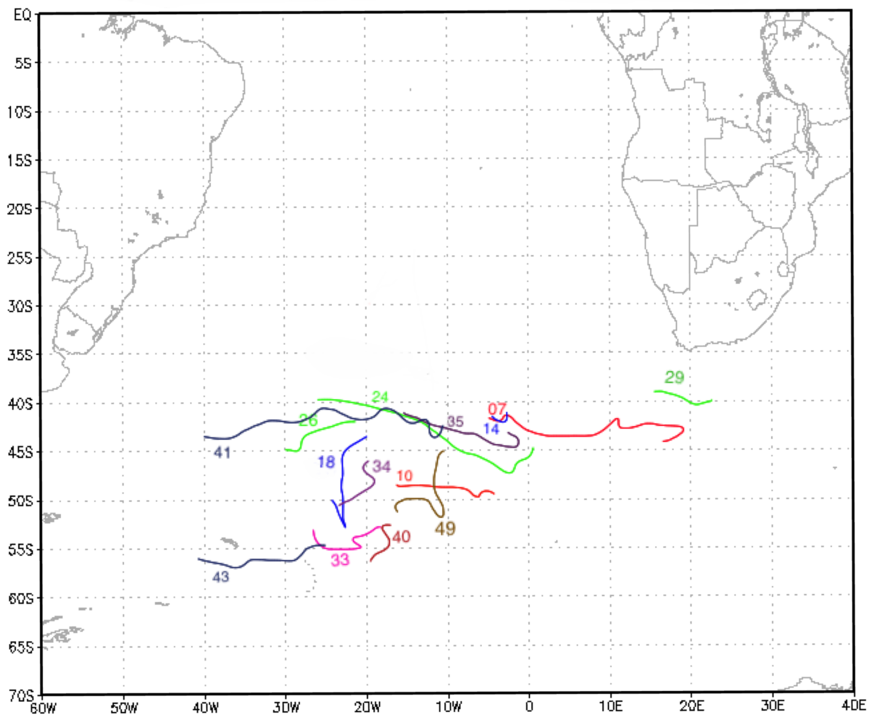

FIG. 4. Trajectories of the cyclones responsible for the 15 events listed at Table 1, occurring in the South Atlantic. The central position of the area with maximum surface speed, if greater than 20 m s^{-1} , is used to track each trajectory.

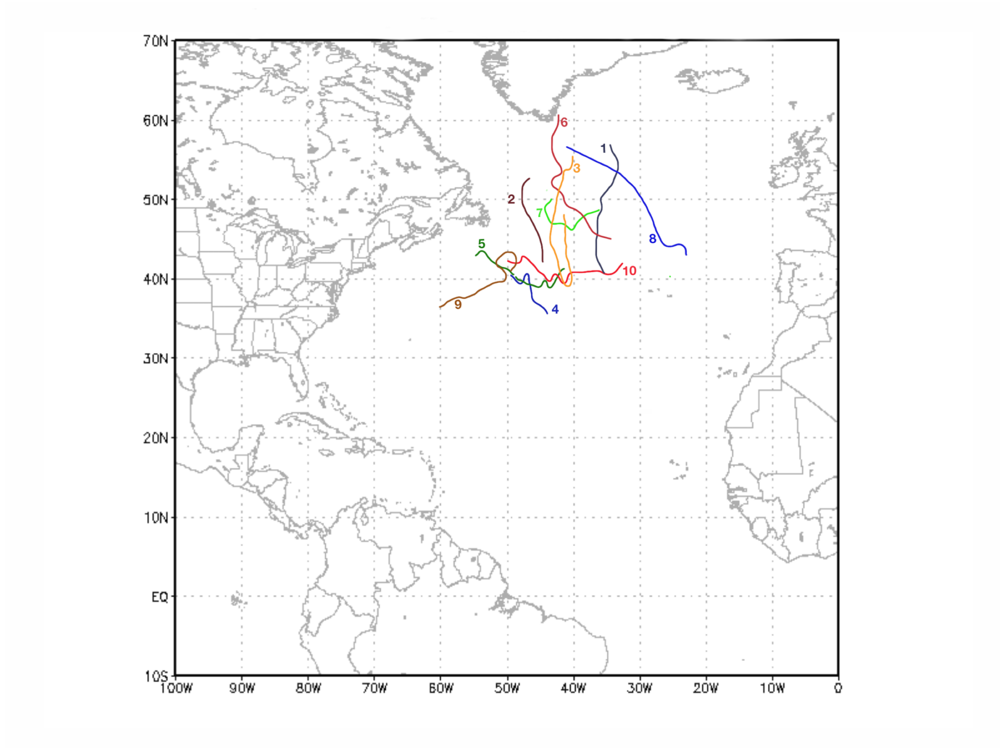

FIG. 5. As in Fig. 4, but for the 10 first events listed in Table 2, occurring in the North Atlantic.

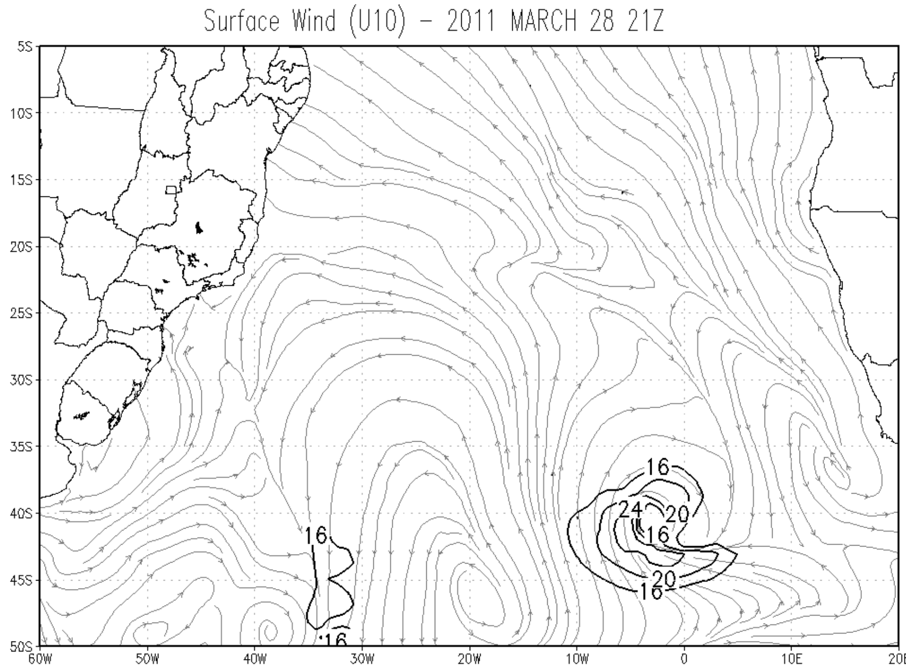

FIG. 6. Contours of surface wind speed U_{10} (m s^{-1}) and streamlines at 2100 UTC 28 March 2011.

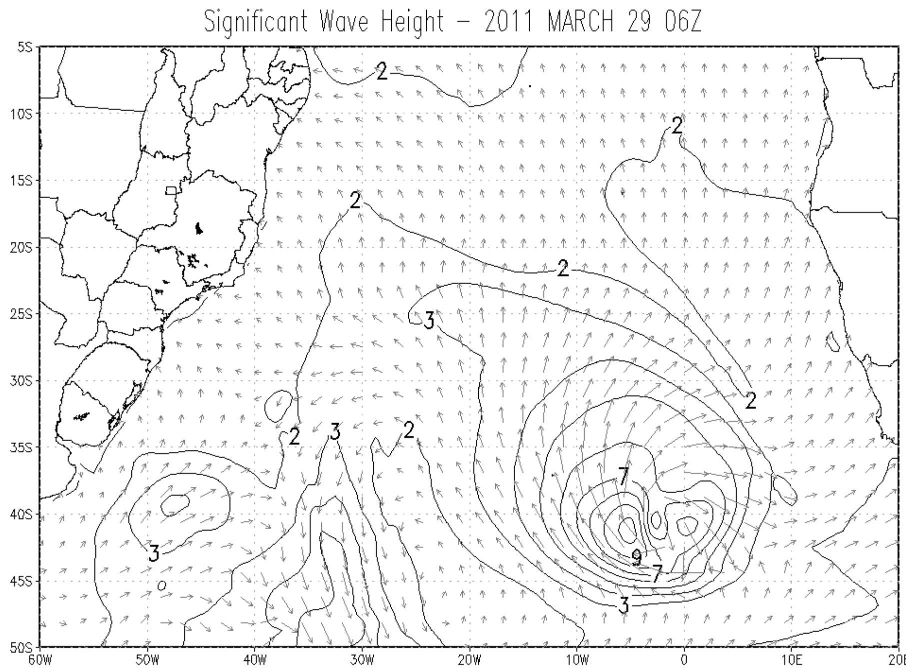

FIG. 7. Significant wave height H_S (m) and mean wave direction at 0600 UTC 29 April 2011.

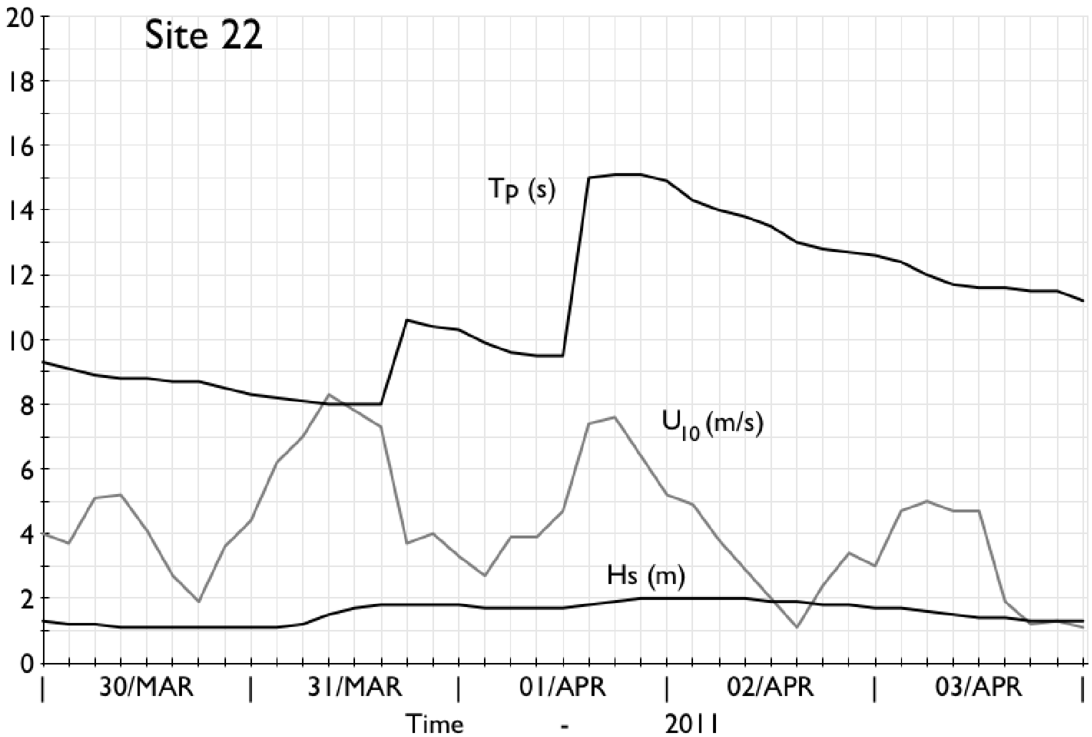

FIG. 8. Time evolution of significant wave height H_S (m), wind speed U_{10} (m s^{-1}), and peak period T_p (s) at site 22, from 30 March to 03 April 2011.

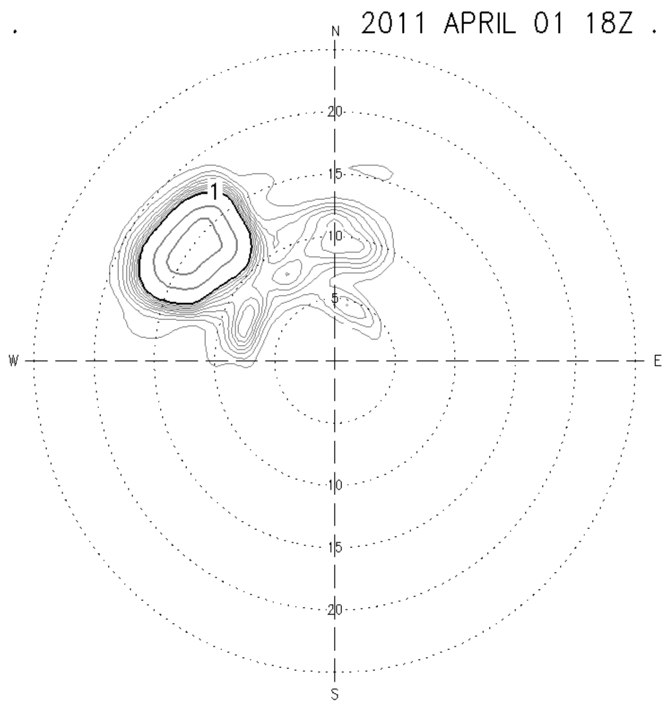

FIG. 9. Spectrum for the site 22 at 1800 UTC 01 April 2011. The units are m^2s rad^{-1}. The plotting interval is 0.1, 1, and 10 for contours smaller than 1, 10 and 100, respectively. The circle represents the period (s). The convention for propagation direction is from the center towards the plotted contour.

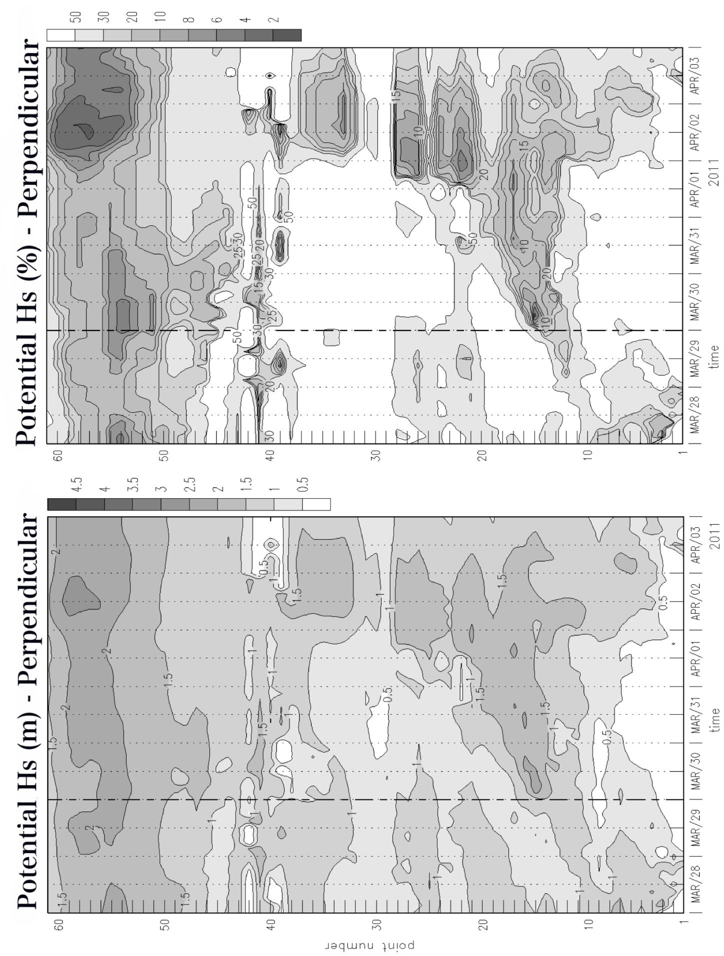

FIG. 10. Hovmöller diagram for the 61 sites of the perpendicular component of the potential significant height H_{SP}^{per} (m), from 28 March to 03 April 2011, in (a) meters and (b) percentile (%). The vertical dashed line delimits the forecast period, starting at 00 UTC 30 March 2011.

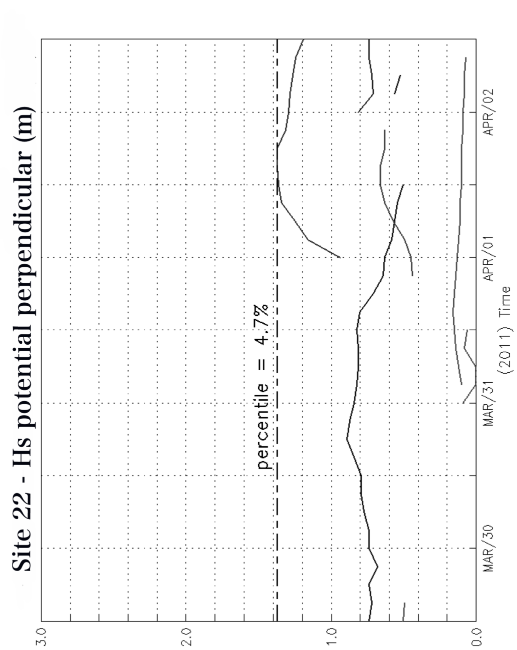

FIG. 11. Time evolution of the perpendicular component of the potential significant height H_{SP}^{per} (m) for individual wave systems (WS), from 30 March to 02 April 2011. The horizontal dashed line indicates the percentile of the strongest H_{SP}^{per} during the 4-day period.

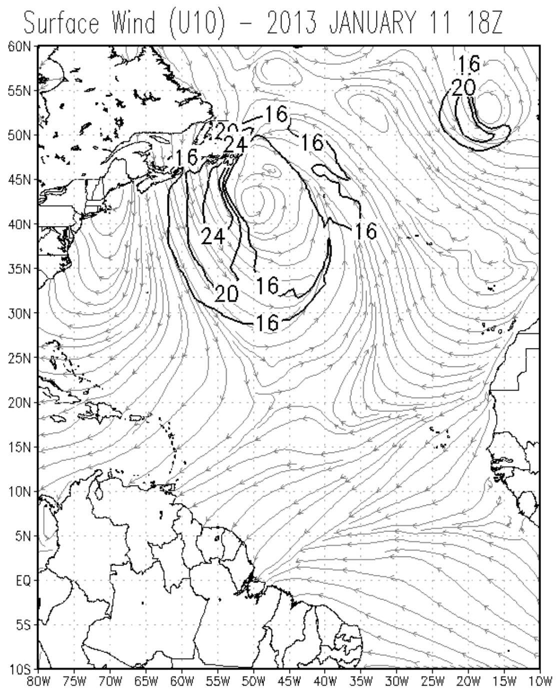

FIG. 12. Wind field U_{10}, as in Fig. 6, but at 1800 UTC 11 January 2013.

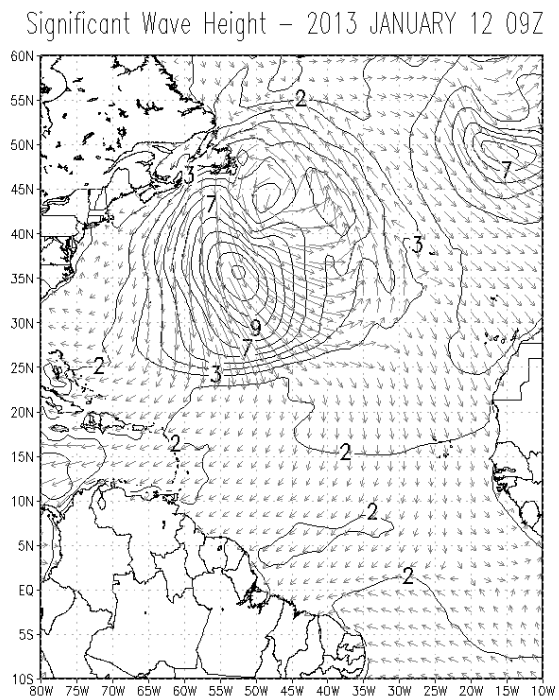

FIG. 13. Significant wave height H_S, as in Fig. 7, but at 0900 UTC 12 January 2013.

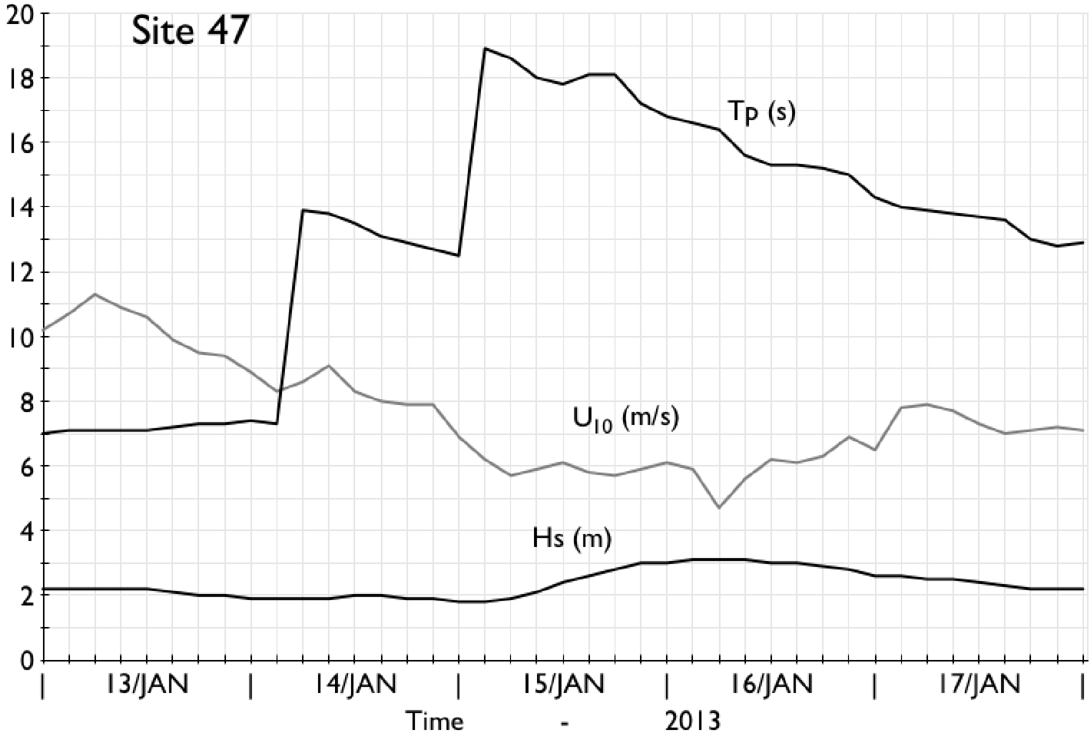

FIG. 14. Time evolution as in Fig. 8, but at site 47, from 13 to 17 January 2013.

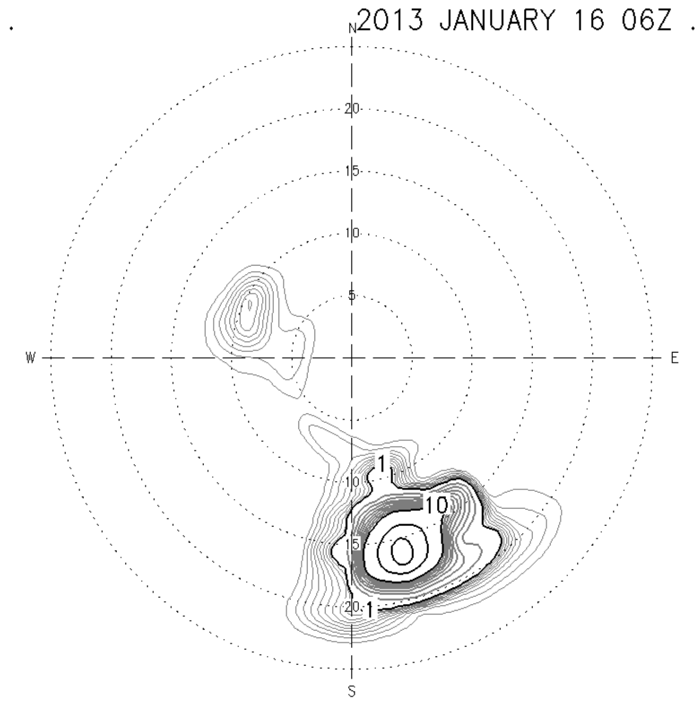

FIG. 15. Spectrum as in Fig. 9, but for the site 47 at 0600 UTC 16 January 2013.

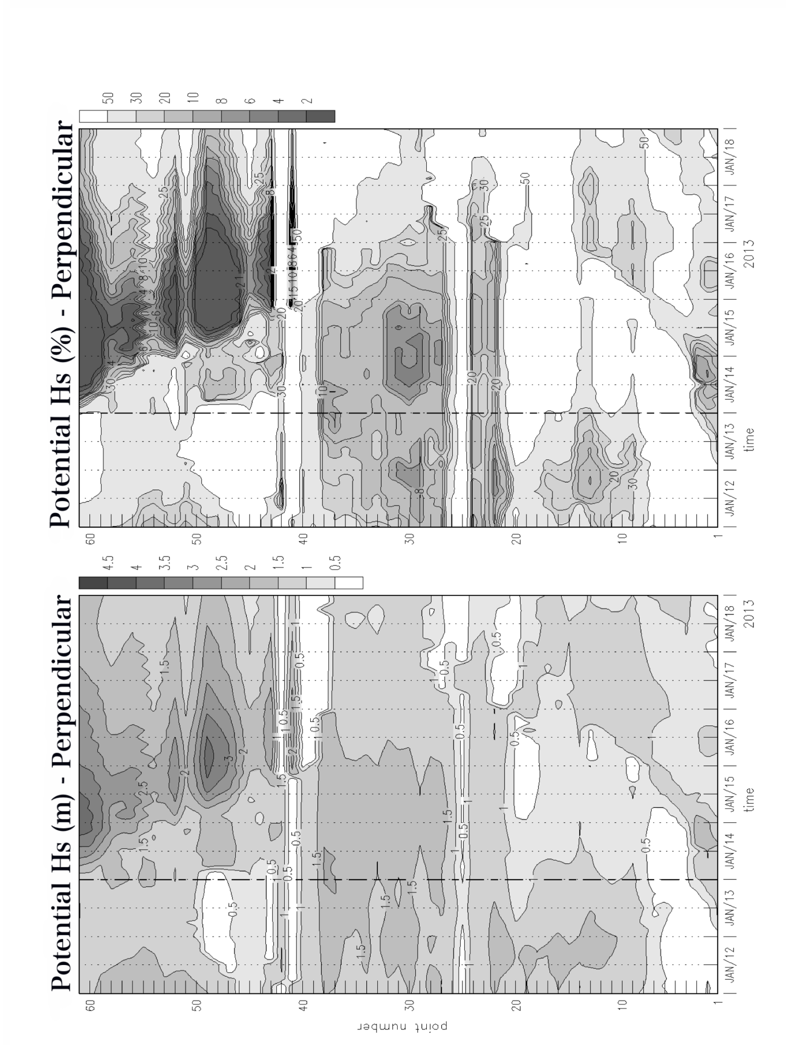

FIG. 16. Hovmöller diagram for H_{SP}^{per} and its percentile, as in Fig. 10, but from 12 to 18 January 2013. Forecast starting at 00 UTC 14 January 2013.

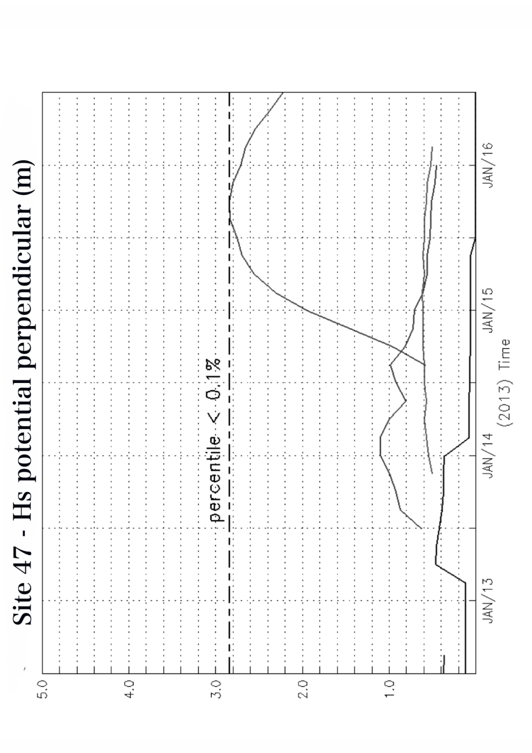

FIG. 17. Time evolution of H_{SP}^{per} for the wave systems, like Fig. 11, but at site 47 from 13 to 16 January 2013.

Tables

event	date	H_S	H_{SP}	H_{SP}^{per}
7	1986 06 02	1.7	2.00	1.99
10	1990 08 13	1.6	1.97	1.83
14	1986 05 31	1.4	1.72	1.71
18	1998 05 18	1.6	1.95	1.57
24	1979 08 01	1.4	1.57	1.46
25	1980 03 17	1.4	1.75	1.40
26	1979 08 08	1.2	1.49	1.38
29	2007 06 10	1.2	1.37	1.36
33	1983 09 16	1.7	2.11	1.30
34	1996 08 23	1.7	2.09	1.30
35	2004 10 18	1.2	1.39	1.29
40	1982 06 09	1.5	1.55	1.24
41	1984 07 12	1.2	1.31	1.22
43	2003 05 25	1.6	1.92	1.19
49	1992 03 07	1.2	1.40	1.12

TABLE 1. Cases with significant wave height $H_S \leq 1.8$ m selected from the 50 cases for the site 22 presented in Fig.3a. The first column refers to the event number presented in the figure. The properties shown are significant wave height (H_S), potential significant wave height (H_{SP}), and its component perpendicular to the coast (H_{SP}^{per}).

event	date	H_S	H_{SP}	H_{SP}^{per}
1	1982 02 08	3.7	4.19	3.95
2	1983 12 27	3.4	3.92	3.69
3	1985 12 07	2.9	3.36	3.17
4	2009 12 31	2.8	3.34	3.15
5	1982 01 05	3.0	3.59	2.96
6	1996 12 24	2.7	3.10	2.92
7	2005 10 18	2.5	3.09	2.91
8	1989 11 23	2.3	2.86	2.85
9	2010 02 10	2.8	3.36	2.77
10	1985 02 09	2.3	2.92	2.75

TABLE 2. Main properties, as in Table 1, but for the first 10 cases presented at Fig.3b.